The role of drifts on the isotope effect on divertor plasma detachment in JET Ohmic discharges

V. Solokha¹, M. Groth¹, S. Brezinsek², M. Brix³, G. Corrigan³, C. Guillemaut⁴, D. Harting³, S. Jachmich⁵, U. Kruezi⁶, S. Marsen⁷, S. Wiesen² and JET contributors*

¹ Aalto University, P.O. Box 14100, FI-00076, Aalto, Espoo, Finland
² Forschungszentrum Jülich GmbH, Institut fur Energie- und Klimaforschung, IEK-4 - Plasmaphysik, 52425 Julich, Germany

³ EUROfusion Consortium, JET, Culham Science Centre, Abingdon, OX14 3DB, UK
 ⁴ Instituto de Plasmas e Fusao Nuclear, Instituto Superior Tecnico, Lisbon, Portugal
 ⁵ Ecole Royale Militaire School, Av de la Renaissance 30, Brussels, Belgium
 ⁶ ITER Organization Route de Vinon sur Verdon, Saint Paul-lez-Durance, France
 ⁷ Max-Planck-Institute for Plasma Physics, Greifswald, Germany
 * See the author list of E. Joffrin et al. 2019 Nucl. Fusion 59 112021

Corresponding author email: vladimir.solokha@aalto.fi

Abstract

Experiments in JET-ILW Ohmic confinement mode plasmas show that the line-averaged detachment onset density in deuterium discharges is approx. 10% lower than in hydrogen discharges. The magnitude of the isotope effect on the detachment onset density depends on the divertor geometry, the magnetic configuration and the throughput of the sub-divertor/divertor cryopump system. Simulations with the edge fluid code EDGE2D-EIRENE revealed that the pumping of neutral gas within the JET divertor is effective near the outer divertor target only. The studies show that the magnitude of the isotope effect is determined by the molecular pressure in the sub-divertor pumping plenum.

According to the simulations, operating in vertical configurations or closer proximity of the strike point increases the molecular pressure (and thus throughput) in front of the outer pumping plenum by up to 15% compared to the horizontal configuration, thus producing a stronger isotope effect on the detachment onset density. Similarly, EDGE2D-EIRENE predicts that plasma, hence neutral, redistribution due to $E \times B$ drifts in favourable B_T configurations (ion $B \times \text{grad}(B)$ towards the divertor) decreases the throughput. The total decrease of the throughput reduces the isotope effect on the detachment onset density, and decreases the detachment onset density for both isotopes.

1. Introduction

Present-day tokamak designs call for highly dissipative boundary plasmas that can exhaust more than 80% of the power leaving the core plasma before it reaches the divertor targets [1]. The reduction of the heat flux to the target plates in high-density, detached divertor conditions was

demonstrated for most major tokamaks [2-11]. In detached divertors, the heat fluxes to the divertor target plates within the material limits (<10 MW/m²) were observed. The onset of detachment is caused by a combination of volumetric momentum and power losses due to plasma-atom and plasma-molecule interaction, e.g., by the collisional processes such as charge-exchange and the line radiation. These processes take place at plasma (electron, T_e) temperatures below 3 eV, at which the collisional ionisation rate is reduced and the recombination rate increased dramatically [12,13]. The ionisation mean free path (MFP) of recycled atoms is typically much shorter than the dimensions of the divertor, therefore most of the atoms are re-ionized before reaching the core plasma [14].

The current of molecules removed by the cryopump is determined by the molecular pressure at the cryopump, which depends on the divertor plasma conditions and the divertor geometry [15]. The wall retention rate of the JET-ILW is typically more than 10 times smaller than the cryopump pumping rate [16]. The gas conductance between the inner pumping plenum and the cryopump is significantly lower than the conductance between the outer pumping plenum to the cryopump, thus making pumping at the inner divertor leg insignificant. In the vertical-horizontal (V5/C) configuration at JET (Fig. 1), the probability of a molecule ejected from the inner strike point (ISP) to reach the cryopump is approximately 30 times lower than for a molecule ejected from the outer strike point (OSP). The cryopump is located at the outboard side, due to the limited space available on the inboard side. In JET the cryopump is connected to the divertor chamber via two pumping plena in the inner and outer divertor corners. This difference in conductance of the inner target (IT) and outer target (OT) pumping plena affects the divertor molecular density. The edge line-averaged electron density has been used as a proxy for the outer-midplane separatrix electron density to determine the detachment onset density. The measurements of the edge line-averaged density are done by the far-infrared interferometry [17].

In JET, the isotope effect on the detachment onset density was extensively investigated in the 1998 DTE campaign [18], indicating a 30% higher detachment onset density for the hydrogen L-mode pulses in the vertical target configuration of the JET-C than for the deuterium. The JET-C discharges in hydrogen exhibited the effective charge approx. 1.5, while the deuterium showed 2.0 due to the higher physical sputtering rate (no isotope effect on the chemical sputtering was found in L-mode JET plasmas), the deuterium and tritium plasmas showed an insignificant difference in effective charge [18]. The C^{III} photon yield of the hydrogen discharges was reported 2-3 times lower than in the deuterium shots. Hence, impurities affected the divertor plasma conditions in the JET-C. On the other hand, the Ohmic pulses in JET-ILW typically have an effective charge close to unity [19]. Therefore, the role of the impurities on the isotope effect is assumed small. While the numerical investigation of the isotope effect in JET-ILW by J. Uljanovs et al. [20] did not include the effects of cross-field drifts and currents, this paper describes EDGE2D-EIRENE [21-24] simulations of the isotope effect in JET-ILW Ohmic discharges without nitrogen seeding with realistic sub-divertor geometry [25], including drift effects.

2. Experimental Results

The isotope effect was investigated in JET-ILW Ohmic discharges with plasma currents, I_P of 2.0 MA, and on-axis magnetic toroidal fields, B_T of 2.0 T with the ion $B \times \text{grad}(B)$ drift towards the divertor (favourable direction) in the V5/C and VV configuration. Two types of fuelling were used: density steps and a fuelling ramp. The density steps were used for measuring the steady-state sub-divertor pressure and usage of SP sweeps for the Langmuir probes profile reconstruction. The response time of the subdivertor pressure measurements to gas fuelling change was $t_{eq} = 0.2$ s for V5/C and $t_{eq} = 0.5$ s for VV configuration. Fuelling ramps were used to capture the rollover with high time resolution.

The lighter hydrogen isotopes result in higher rollover densities compared to the deuterium (Fig. 2). In the vertical-horizontal configuration, the isotope effect is 10%. The vertical-vertical configuration exhibits the same isotope effect equal to 30%. For the same line-averaged density, the hydrogen plasma has 50% higher temperatures and lower densities than the deuterium plasma along the outer target.

For the same upstream electron density and electron temperature, the sub-divertor pressure in hydrogen discharges was observed to be 50% lower than in equivalent deuterium pulses (0.04 Pa in H_2 , 0.06 Pa in D_2 at $\langle n_e \rangle = 2.2 \times 10^{19}$ m⁻³). The difference in the subdivertor pressure can be caused by the isotope effect on the saturation pressure and the conductance. The sub-divertor pressure is measured with a capacitance manometer (baratron) [24], thus independent of the gas species. The conductance of the pumping plenum and pumping speed scale linearly as the thermal velocity of the molecules (Eq.1).

(1)
$$S_{eff} = A p_s v_{th} / 4$$

Where A - area, p_s - sticking probability, v_{th} - thermal velocity.

On the other hand, the lighter isotope was found to have higher vapour pressures for a fixed temperature than heavier isotopes [28], which decreases the sticking probability of gases on the actual cryopump panels. As was investigated in [29], the effective albedo, the probability for molecules to be reflected in the opposite direction, ($\alpha = 1-p_s$) of the louvre is approx. 0.8, which significantly reduces the throughput. The louvres are located between the core plasma and the cryopump. The louvres albedo is considerably higher than albedo of cryopump [22] implying that the sub-divertor pressure is governed by the cryopump sticking probability. On the other hand, the divertor neutral density is affected by fuelling and plasma parameters only. Therefore, the sub-divertor pressure cannot be used as a proxy for the divertor neutral density in these plasmas.

The difference in pumping speed of the combined pumping plenum conductance and cryopump between hydrogen and deuterium was estimated using the ratio of the fuelling current and the sub-divertor pressure in density step discharges. Despite the higher sticking probability in the deuterium case [28], the pumping speed ratio was estimated to be $S_H/S_D=1.2$. In the case of equal albedo ($\alpha_H = \alpha_D = 0.92$), as shown in [29], the pumping speed ratio is expected to be $S_H/S_D=\sqrt{m_D}/\sqrt{m_H}=1.41$. Hence, the pumping plenum's conductance plays a more dominant role in the throughput, compared to the cryopump. In the case of equal fuelling current, the case with low pumping speed has higher neutral densities.

The difference in the measured outer midplane electron density profiles for H and D is less than 15% at $\langle n_e \rangle = 1.7 \times 10^{19}$ m⁻³ (Fig. 3a), which is comparable with the systematic errors of the electron density estimation from the Thomson scattering (TS) and interferometry diagnostics. Electron temperature profiles for H and D are identical (Fig. 3b).

3. Numerical Simulations Results

The EDGE2D-EIRENE simulations utilized a magnetic configuration from JET pulse number 80295 in the V5/C configuration representing all of the experiments for pure hydrogen and deuterium plasmas. The grid includes the main plasma volume, the divertor, and the sub-divertor region. Simulations of hydrogen and deuterium plasmas with sputtered beryllium were conducted. EIRENE considered the elastic collisions of hydrogen atoms/molecules with ions [30]. However, the molecular-molecular and atomic-atomic collisions were not included in the EIRENE simulations because the approximate Knudsen number at the pumping plenum is below unity for the sub-divertor pressure range in Ohmic discharges. To eliminate the influence of the cross-field transport in the first step of analyses (Fig. 4), the hydrogen and deuterium cases had equal particle and heat diffusion coefficients, results with different diffusion coefficients are presented in the discussion section. The diffusion coefficients were used the same as for the hydrogen case in [31]. The cryopump albedo value for both isotopes was assumed to be $\alpha = 0.92$. All simulations included E × B drifts and curvature drifts.

The cryopump is located near the outer target and behind the pumping plenum which protects the cryopump from the radiation (Fig. 1). The shortest path length from the outer pumping plenum to the cryopump is approximately 30 cm, while the path from the inner pumping plenum to the cryopump is greater than 120 cm. According to [32], this difference in molecular path length is sufficient to raise the effective albedo of IT pumping plenum from 0.8 to 0.95. For the presented cases, the effective (calculated using EIRENE) albedo of the outer pumping plenum is approximately 0.8. The inferred IT pumping plenum's albedo is approximately unity.

The recycled particles from IT and OT enter the inner and outer pumping plena, correspondingly. D. Moulton et al. [33] showed that the contribution of the IT neutrals to OT ionisation source is negligible. And S. Varoutis et al. [34] stated that the neutral recirculation through the gaps of the vertical divertor tiles is two orders of magnitude less than recycling flux.

In the simulations, the throughput was decreased by 5-15% due to the $E \times B$ drift towards the IT compared to cases without drifts. In particular, the radial $E \times B$ drifts move the ions towards the

inner sub-divertor entrance in the favourable B_T direction and diminish pumping capacity by raising the molecular pressure at the inner sub-divertor entrance and decreasing the molecular pressure near the outer sub-divertor entrance (Fig. 5).

The EDGE2D-EIRENE predicted molecular and electron densities are 15% higher at the OT in the case without drifts, and the electron density profile at the OT is shifted by approx. 3 cm towards the outer target pumping plenum (Fig. 6), increasing the throughput difference between the isotopes by increasing the number of molecules reflected towards the cryopump. The decreased neutral and electron densities cause lower momentum losses in hydrogen cases than in the deuterium cases.

The influence of the ionisation mean free path difference on the divertor conditions was small in comparison with the influence of the pumping plenum conductivity difference. Dedicated EIRENE simulations with a fixed background plasma showed higher deuterium densities in the divertor region (by 20-30%), while the hydrogen atoms penetrate the core plasma deeper than deuterium atoms.

The detachment onset density for both isotopes was predicted to be approx. 5% lower in simulations with the drifts turned on than for the case without drifts (Fig. 7a). The predicted sub-divertor pressure in the case without drifts is 10% higher than in the case of the favourable B_T case and therefore the current to the pump is also higher at rollover densities (Fig. 7b).

To investigate the impact of Be as the primary intrinsic impurity species in JET-ILW, additional EDGE2D-EIRENE simulations were executed assuming Be main chamber walls and a W divertor [35]. As in Harting et al. [35], the main source of Be is the sputtering by charge-exchange atoms from the main chamber walls. The effective sputtering yield of Be (the sputtering yield by a monoenergetic beam with the average ion energy) in the hydrogen case is lower by 60% than in the deuterium case. The total Be radiation (P_{rad} Be) is approx. 5 times lower than the total hydrogen/deuterium radiation, but differences between isotopes result in a 15% lower total radiation in the hydrogen case than in the deuterium case due to the higher Be density. The simulation results are in quantitative agreement with a total radiation power difference of approximately 20% observed in the experiments. Introducing Be as the primary impurity species has a weak impact (<5%) on the divertor electron density and temperature due to the low concentration. The tungsten line-radiation does not play a role in the isotope effect due to low sputtering yields of tungsten in the ohmic discharges; therefore, tungsten transport was neglected.

4. Discussion

In JET-ILW Ohmic plasmas, the experimentally observed and numerically predicted isotope effect on the detachment onset density are of the order 10%, which is within the uncertainties of the measurements. The observed differences in the detachment onset density are derived from line-averaging interferometry at the outer edge of the plasmas, including the pedestal and the scrape-off layer regions, while the simulations are based on the imposed electron density at the separatrix at the outer midplane. The upstream density profiles for electron density and temperature from the high-resolution Thomson scattering are uncertain in the range of the 10% due to the profile shifting and absolute calibration errors. The uncertainty in the assumed diffusion coefficients changes the total fuelling current and molecular densities.

In the experiment (Fig. 2), the line-integrated density is used as an x-axis value, which is a proxy for upstream separatrix density and depends on the core density. The upstream separatrix density cannot be used in the experimental comparison because the accuracy of the estimation from the TS diagnostic is much lower than the isotope effect. The simulation results comparison used the upstream separatrix density directly (Fig. 8). Thus, the comparison of the experimental and predicted isotope effect requires the measurements of the upstream separatrix density, which has unacceptably low accuracy due to the errors in separatrix position estimation.

A dedicated set of EDGE2D-EIRENE simulations with the more realistic diffusion coefficients for the deuterium in the fav. B_T case exhibited an increase of the detachment onset density by 10% (Fig. 8a and Fig. 8b) in comparison with the hydrogen cases.

To further investigate the impact of cross-field drifts on the isotope effect on the detachment onset density, the EDGE2D-EIRENE simulations of the divertor plasma with the ion $B \times \text{grad}(B)$ drift out of the divertor (unfavourable direction). The numerical experiment quantifies the increase of the throughput caused by $E \times B$ drifts as they move plasma in the direction of the outer pumping plenum. Throughput increases due to the lower outer pumping plenum albedo than inner pumping plenum albedo. Simulations revealed a 30% higher electron and molecular densities at the OT and enhanced (approx. 10%) isotope effect on the detachment onset density. The radial $E \times B$ drifts move the ions towards the outer sub-divertor entrance in the unfavourable B_T (Fig. 9) increasing throughput by 10%.

The isotope effect on detachment onset density between deuterium and tritium is less significant than between hydrogen and deuterium due to the two times lower difference in the square root of mass ratio ($\sqrt{m_T}/\sqrt{m_D} - 1 = 0.22$). Thus, the isotope effect in case of equal diffusion coefficients can be considered negligible. The difference in the detachment onset density caused by the diffusion coefficients is expected to be dominant in deuterium and tritium cases.

The different effective albedos of the inner and outer pumping plena are important in the vertical-horizontal plasma configuration because the recycled neutrals from the inner target

cannot be pumped, while in the vertical-vertical configuration both plena are connected by the private flux region (Fig. 1). Therefore, the role of drifts on the isotope effect is expected to be smaller in the VV configuration.

5. Conclusions

The impact of the conductances of the pumping plena, the sticking coefficients of the divertor cryopump, and the $E \times B$ drift direction influence on the isotope effect of detachment onset density was investigated in this paper. Experimentally, the isotope effect on the detachment onset density is equal to 10% in the V5/C configuration. The effect is partly caused by the increased D_2 density in the divertor due to the difference in the pumping plena conductance compared to H_2 . Tokamak operation in the favourable B_T direction as carried out experimentally in these studies reduces the pumping capacity of the system in the vertical-horizontal configuration compared to omitting cross-field drifts.

In EDGE2D-EIRENE simulations with drifts in the favourable B_T direction, plasmas have decreased throughput and higher molecular densities near the OT strike point. Thus, they are predicted to lead to a weaker isotope effect on the detachment onset density as drifts decrease the detachment onset density for both isotopes. Drifts move plasma density towards the IT pumping plenum leading to a decrease in the throughput. Based on predictions, the isotope effect on the detachment onset density in favourable B_T direction is caused by the outer midplane profile difference and not by the divertor conditions. The dependence of the detachment onset density on the transport coefficients calls for highly accurate experimental and numerical analysis of the upstream profiles (Fig. 8b).

Acknowledgements

This work has been carried out within the framework of the EUROfusion Consortium and has received funding from the Euratom research and training programme 2014-2018 and 2019-2020 under grant agreement No 633053. The views and opinions expressed herein do not necessarily reflect those of the European Commission.

References

[1] R. A. Pitts, et al. (2019) Nuclear Materials and Energy 20 100696

https://doi.org/10.1016/j.nme.2019.100696

[2] A. Kallenbach et al. (2015) Nucl. Fusion 55 05302

https://doi.org/10.1088/0029-5515/55/5/053026

[3] T.W. Petrie et al (1997) Nucl. Fusion 37 321

https://doi.org/10.1088/0029-5515/37/3/I03

[4] T.W. Petrie et al (1997) Nucl. Fusion 37 643

https://doi.org/10.1088/0029-5515/37/5/I07

[5] O. Gruber et al. (1995) Phys. Rev. Lett. 74, 4217

https://doi.org/10.1103/PhysRevLett.74.4217

[6] A. Loarte, et al. (1998) Nucl. Fusion 38 331

https://doi.org/10.1088/0029-5515/38/3/303

[7] G.M. McCracken, et al. (1999) Journal of Nuclear Materials 266-269

https://doi.org/10.1016/S0022-3115(98)00571-6

[8] A. Huber, et al. (2013) Journal of Nuclear Materials 438 S139-S147

http://dx.doi.org/10.1016/j.jnucmat.2013.01.022

[9] A. L. Moser et al. (2020) Phys. Plasmas 27, 032506

https://doi.org/10.1063/1.5109027

[10] J. R. Harrison et al. (2017) Nuclear Materials and Energy 12 1071–1076

https://doi.org/10.1016/j.nme.2016.10.020

[11] A. R. Field et al. (2017) Plasma Phys. Control. Fusion 59 095003

https://doi.org/10.1088/1361-6587/aa764c

[12] A. Yu. Pigarov (2002) Phys. Scr. 2002 16

https://doi.org/10.1238/Physica.Topical.096a00016

[13] A. Tonegawa (2003) Journal of Nuclear Materials Volumes 313–316, Pages 1046-1051 https://doi.org/10.1016/S0022-3115(02)01535-0

[14] Stangeby, P. C. (2000) Plasma Physics and Controlled Fusion, 42(12B), B271–B291.

doi:10.1088/0741-3335/42/12b/321

[15] A. Loarte (2001) Plasma Phys. Control. Fusion 43 R183

doi:10.1088/0741-3335/43/6/201

[16] T. Loarer et al (2013) Journal of Nuclear Materials, 438, Pages S108-S113

http://dx.doi.org/10.1016/j.jnucmat.2013.01.017

[17] J A Fessey et al 1987 J. Phys. E: Sci. Instrum. 20 169

https://doi.org/10.1088/0022-3735/20/2/009

[18] Maggi C. F. et al (1999) Nucl. Fusion 39 979

https://doi.org/10.1088/0029-5515/39/8/303

[19] S. Brezinsek et al, Journal of Nuclear Materials (2015) 463

https://doi.org/10.1016/j.jnucmat.2014.12.007

[20] Uljanovs J. et al (2017) Nucl. Mater. Energy 12 791–7

https://doi.org/10.1016/j.nme.2017.03.028

[21] Simonini R. et al (1994) Contrib. Plasma Phys. 34 368–73

https://doi.org/10.1002/ctpp.2150340242

[22] Wiesen S. and (JET ITC-Report) 2006

(http://eirene.de/e2deir_report_30jun06.pdf)

[23] Fundamenski W. et al (2008) Contrib. Plasma Phys. 48 190-5

https://doi.org/10.1002/ctpp.200810034

[24] Reiter D., Baelmans M. and Borner P. (2005) Fusion Sci. Technol. 47 172–86

https://doi.org/10.13182/FST47-172

[25] Moulton D et al (2015) 42nd EPS Conf. on Plasma Physics O4.119

[26] U. Kruezi et al (2012) Rev. Sci. Instrum. 83, 10D728

https://doi.org/10.1063/1.4732175

[27] Carl Edward Rasmussen and Christopher K. I. Williams The MIT Press, 2006.

ISBN 0-262-18253-X.

http://www.gaussianprocess.org/gpml/

[28] Chr. Day et al (2005) Fusion Science and Technology, 48:1, 29-34

https://doi.org/10.13182/FST05-A873

[29] V. Solokha et al 2020 Phys. Scr. 2020 014039

https://doi.org/10.1088/1402-4896/ab4bed

[30] Kotov, V., Reiter, D., & Kukushkin, A.S. (2007). Numerical study of the ITER divertor plasma with the B2-EIRENE code package (Juel--4257)

[31] A. V. Chankin et al Plasma Phys. Control. Fusion 61 (2019) 075010

https://doi.org/10.1088/1361-6587/ab1629

[32] D. H. Davis (1960) Journal of Applied Physics 31, 1169

https://doi.org/10.1063/1.1735797

[33] D. Moulton et al (2018) Nucl. Fusion 58 096029

https://doi.org/10.1088/1741-4326/aacf0f

[34] S. Varoutis et al (2017) Fusion Engineering and Design 121

https://doi.org/10.1016/j.fusengdes.2017.05.108

[35] D. Harting et al (2013) Journal of Nuclear Materials, 438, S480-S483

https://doi.org/10.1016/j.jnucmat.2013.01.098

Figures

Figure 1:

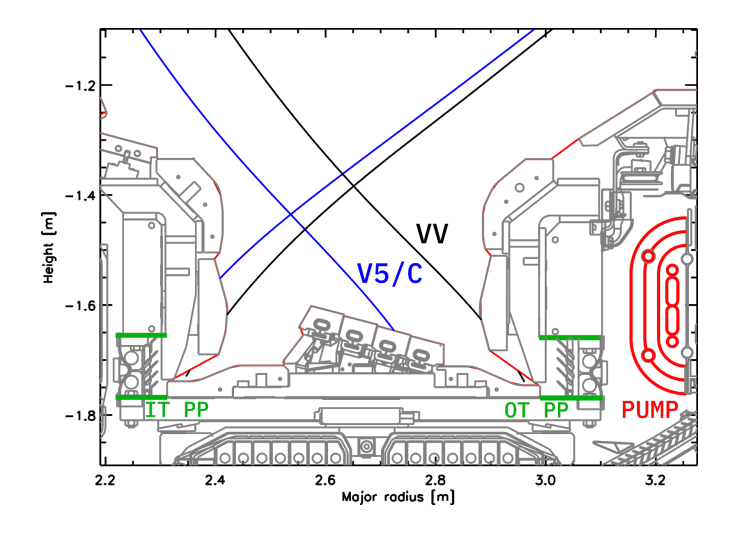


Figure 2:

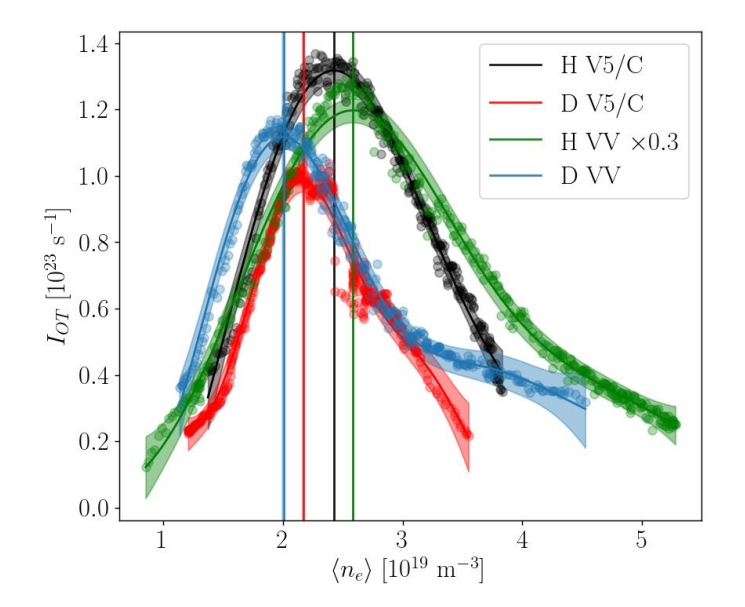


Figure 3:

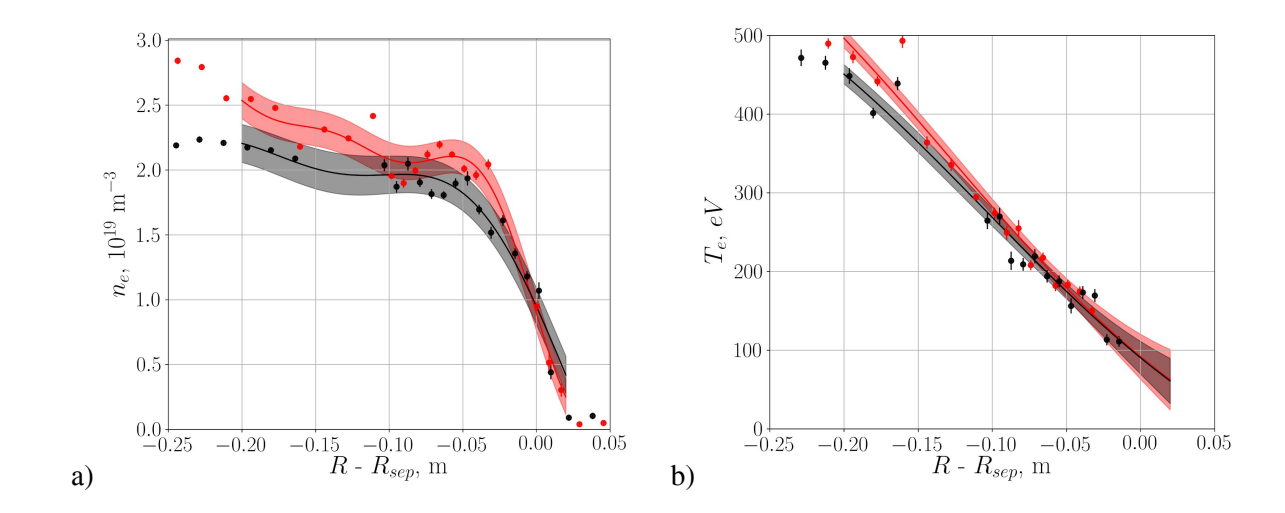


Figure 4:

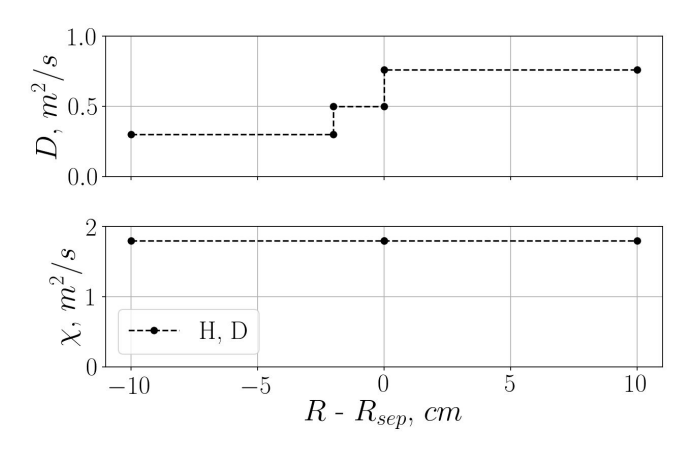


Figure 5:

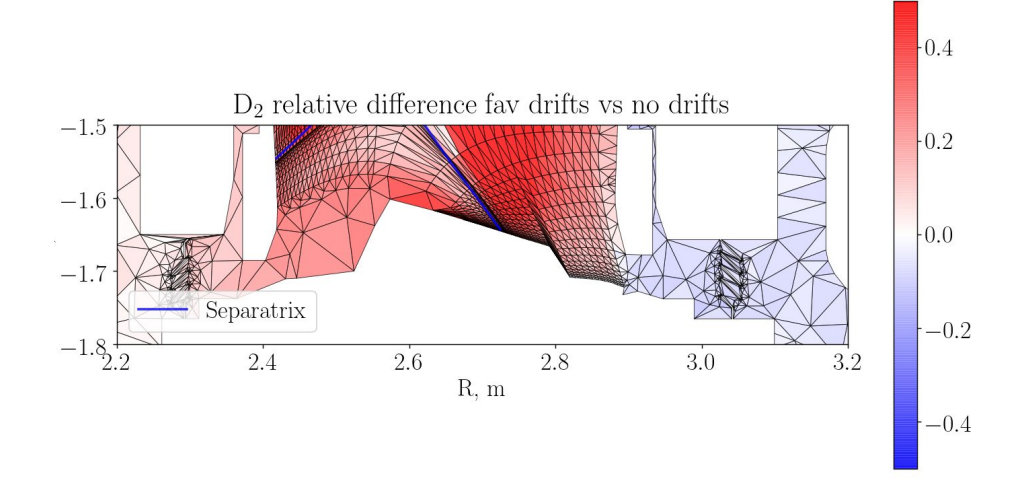


Figure 6:

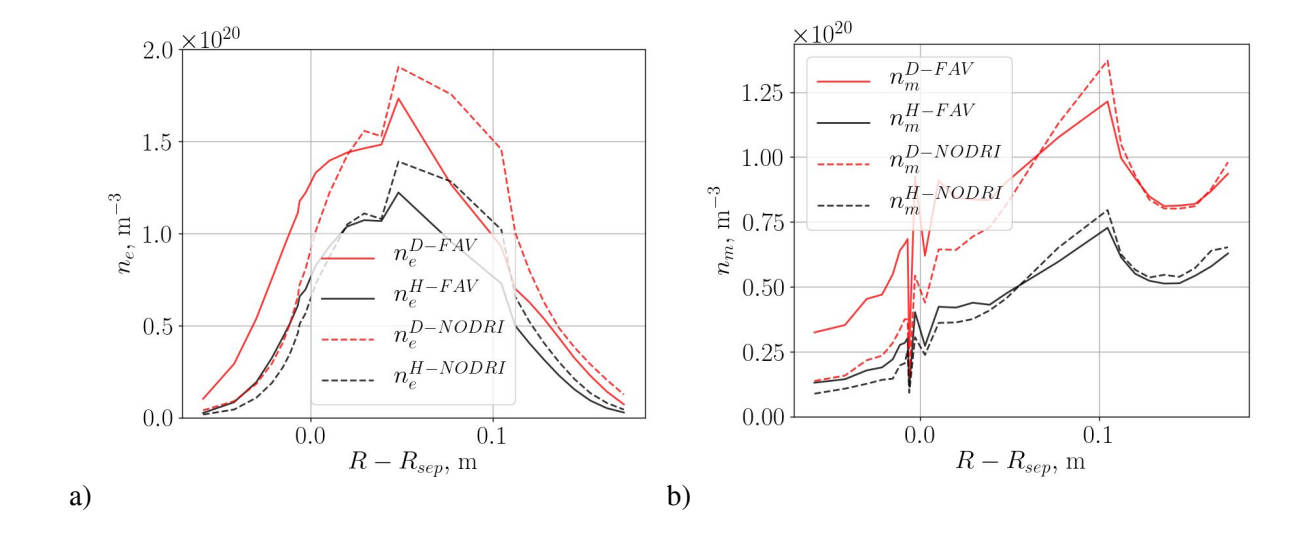
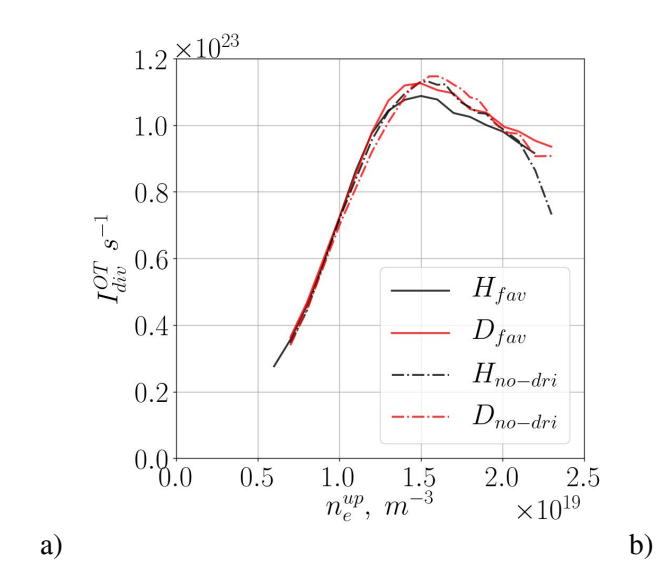


Figure 7:



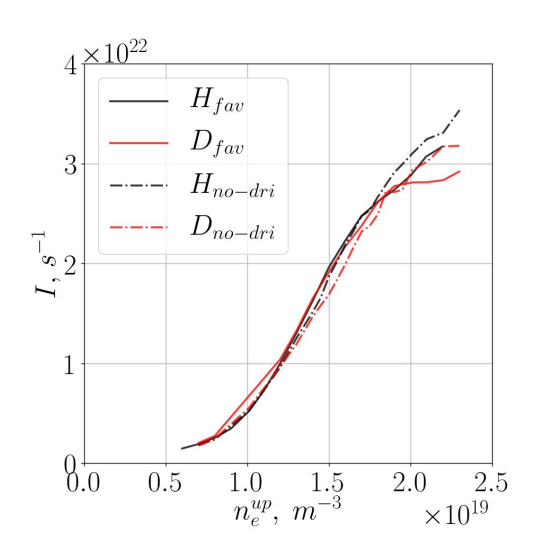
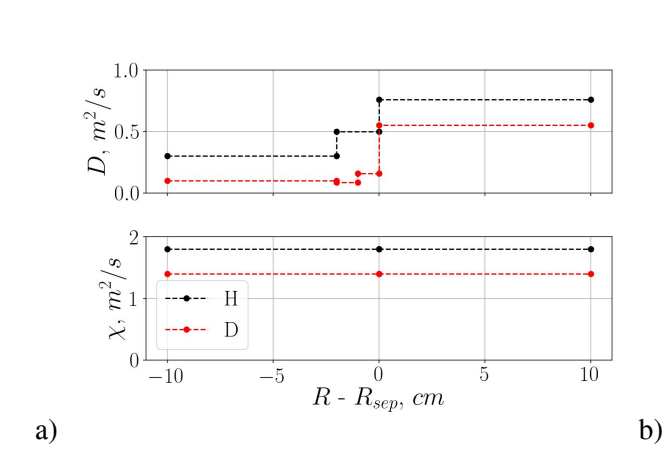


Figure 8:



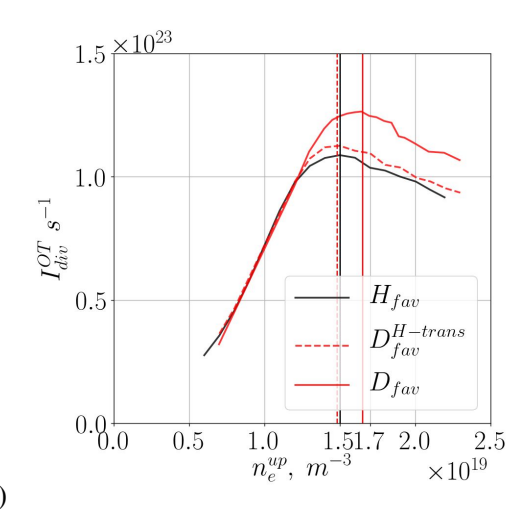


Figure 9:

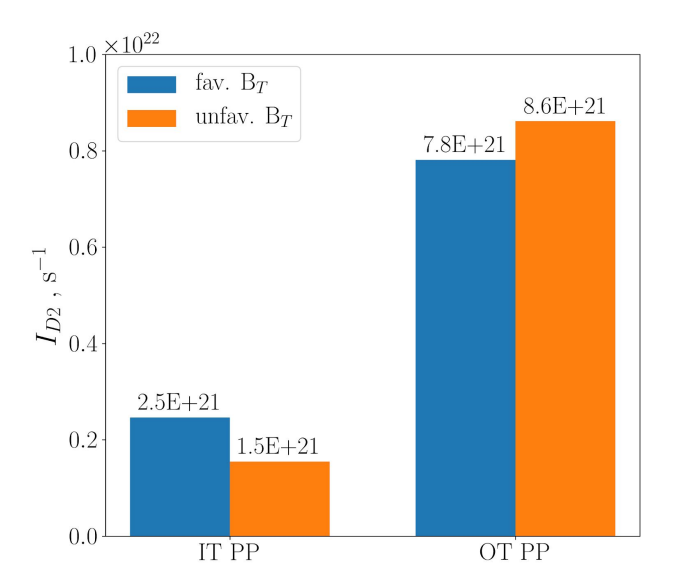


Figure captions:

- **Figure 1:** The separatrix position for vertical-horizontal (V5/C) and vertical-vertical (VV) configurations in the JET divertor with the pumping plena (IT PP and OT PP) and cryopump (PUMP).
- **Figure 2:** The total ion current as a function of the line-averaged edge density. Gaussian Process Regression [27] was used to smooth the experimental data and to determine the value of the rollover taken to be the detachment onset density. The data from the hydrogen discharge in the vertical-vertical configuration was scaled.
- **Figure 3: a)** Outer midplane TS electron density profile (hydrogen black, deuterium red). Gaussian Process Regression [27] has been used to smooth the curve.
- **b**) Outer midplane TS electron temperature profile (hydrogen black, deuterium red). Gaussian Process Regression [27] has been used to smooth the curve.
- **Figure 4:** Assumed particle and heat diffusion coefficients for the hydrogen and deuterium ions as a function of distance from the separatrix at the outer midplane in EDGE2D-EIRENE.
- **Figure 5:** 2D distribution of the relative difference of the D_2 densities in fav. B_T drift and no drift cases at upstream density $n_{e,up} = 1.8 \times 10^{-19} \text{ m}^{-3}$. The blue line is the separatrix contour.
- **Figure 6:** a) Electron density profiles at the OT as a function of distance to the separatrix for the simulation cases at the upstream density $n_{e,up} = 1.8 \times 10^{-19} \text{ m}^{-3}$.
- **b)** Molecular density profiles at the OT as a function of distance to the separatrix for the simulation cases at the upstream density $n_{e,up} = 1.8 \times 10^{-19} \text{ m}^{-3}$.
- **Figure 7: a)** Predicted total ion saturation current as a function of the upstream separatrix density in the fav. B_T and no drift cases.
- **b)** Predicted pumped current as a function of the upstream separatrix density in the fav. $B_{\scriptscriptstyle T}$ and no drift cases.
- **Figure 8: a)** Assumed particle and heat diffusion coefficients at outer midplane for EDGE2D-EIRENE simulations used from [31].
- **b)** Total ion saturation current as a function of the upstream separatrix density and transport coefficients.
- **Figure 9:** The molecular current to the inner target pumping plenum (IT PP) and the outer target pumping plenum (OT PP) for the simulation cases at the upstream density $n_{e,up} = 1.8 \times 10^{-19} \text{ m}^{-3} \text{ in fav. } B_T \text{ (blue)}$ and unfav. $B_T \text{ (orange)}$ drift cases.